Supporting Information

Solar Evaporator Based on Hollow Polydopamine Nanotubes with All-in-One Synergic Design for High-efficient Water Purification

Dan Huang, Jie Zhang, Gang Wu, Si-Chong Chen*, Yu-Zhong Wang

Collaborative Innovation Center for Eco-Friendly and Fire-Safety Polymeric Materials

(MoE), College of Chemistry, Sichuan University, Chengdu 610064, China

Corresponding author. E-mail: chensichong@scu.edu.cn.

Section S1. Supplementary methods

Section S1.1. Fabrication procedure

Section S1.1.1. Preparation of PLA-NF and PDA@NF

5wt% PLA was dissolved in a mixed solvent of trifluoroethanol and trichloromethane (v:v=2:1) to prepare the precursor solution stirring 12 h for electrospinning. The electrospun parameters were set as follows: the flow rate was 0.2 mm/min, the voltage applied was 18.0 kV, and the inner diameter of needle was 0.21 mm. Then the as-spun PLA-NF were vacuum-dried at 50°C.

HCl-Tris buffer solution (pH 8.5, 50 mM) of dopamine hydrochloride with a concentration of 1 g/L was prepared. The PLA-NF was then immersed into the buffer solution for 24 h and 36 h at 25 °C to obtain PDA@NF with different thickness of PDA coating recorded as PDA_{50}@NF and PDA_{100}@NF, respectively. Finally, the PDA@NF membranes were rinsed with deionized water and ethanol respectively before vacuum-drying.

Section S1.1.2. Preparation of PDA-t@PU.

To obtain a solar evaporator with optimal performance for water purification, we explored the preparation conditions of the PDA-t@PU, including the addition amount of PDA-t, the time of dissolving PDA@NF by solvent and the thickness of PU foam matrix.

Firstly, PDA_{50}@NF were immersed in a mixture of ethanol and trichloromethane (v:v=1:1) 24 h to obtain PDA_{50}-t. Then PU foam was immersed in ethanol that dispersed with different amounts of PDA-t, and was oscillated in the shaker to volatilize solvent until the sample was dry with the shaker speed of 90 rpm and the temperature of 40℃, getting PDA_{50}-t@PU with different PDA-t addition of 15 wt%, 25 wt% and 30 wt%.

In order to explore the effect of solvent treatment time, the PDA_{50}@NF was treated in mixed solvent for 24 h, 48 h, 72 h and 96 h, and the PDA_{50}-t@PU-24/48/72/96 h samples were prepared by fixing the addition amount of 30 wt%.

Fixing the addition amount of 30 wt% and the solvent treatment time of 48 h, change the thickness of PU foam from 0.4 to 1.2 cm to explore the effect of sample

thickness.

Finally, according to the SVG rate, the optimized preparation conditions were as follows: the addition amount was 30 wt%, the solvent treatment time was 48 h, the thickness of the sample was 0.7 cm. Moreover, PDA$_{100}$@NF was also prepared under the above optimized preparation conditions to obtain PDA$_{100}$-t@PU.

Section S1.2. Melting behavior water in PDA-t@PU

During the DSC measurement of the melting behavior of water in PDA-t@PU and other control samples, the wetted samples was closely sealed in an Al crucible to prevent the evaporation of water and kept at -30 °C for 5 min to be fully frozen. Then the measurement was performed with scans at linear heating rate 2 °C/min under nitrogen flow flux (50 mL/min), in the temperature ranging from -30 to 30 °C.

Section S1.3. Calculation of energy efficiency.

The energy efficiency (η) of SVG can be calculated by the following eq1:

$$\eta = mE_{equ}/C_{opt}P_0 \tag{1}$$

where m is the mass flux while reaching steady state condition, E_{equ} is the equivalent vaporization enthalpy of the water in samples, P_0 is the solar irradiation power of 1 sun (1 kW m^{-2}), and C_{opt} refers to the optical concentration on the absorber surface.

Section S1.4. Calculation of vapor generation via dark experiment.

The water and samples with the same superficial area were synchronously set in a closed container together with the supersaturated potassium carbonate solution (enabling stabilized RH of ca. 50%) under a temperature of ca. 25 ºC and ambient air pressure. The equivalent evaporation enthalpy (E_{equ}) of water in samples can be estimated by vaporizing the water with identical power input (U_{in}) following eq1:

$$U_{in} = E_0m_0 = E_{equ}m_g \tag{2}$$

Where E_0 and m_0 are the evaporation enthalpy and mass change of bulk water; m_g is the mass change of samples. The energy efficient is also calculated based on E_{equ} of corresponding samples.

Section S1.5. DSC measurement of evaporation enthalpy

In order to prove that the evaporation enthalpy of water in PDA-t@PU was reduced, DSC measurement was carried out to measure the vaporization energy of pure water and water in various samples. During the evaporation enthalpy measurements, the wetted samples was placed in an open Al crucible and measured with linear heating rate 5 °C/min, under nitrogen flow flux (50 mL/min), in the temperature ranging from 20 to 180 °C.

Section S2. Supplementary figures

Section S2.1. Optimization of preparation conditions

As shown in **Figure S1**A-C and A1-C1, the average diameter of as-spun PLA-NF fibers is 530 nm, and the diameter increased to about 620 and 740 nm after PDA coating for 24 h and 36 h. Hence the thickness of PDA shell is estimated to be about 50 and 100 nm, respectively.

With the increase of PDA-t addition, the SVG rate increase gradually, and the evaporation rate is 1.79 kg m^{-2} h^{-1} with the addition amount of 30 wt%. With the increase of solvent treatment time, the SVG rate increases first and then decreases, and the SVG rate reaches 2.1 kg m^{-2} h^{-1} with the treatment time of 48 h. The sample thickness has little effect on SVG rate in the range from 0.4 to 1.2 cm. Furthermore, it can be seen from the SEM diagram that when the treatment time is short, the internal fibers are not completely etched and can't form a hollow structure, while obvious hollow structure can be observed when the treatment time is further increased.
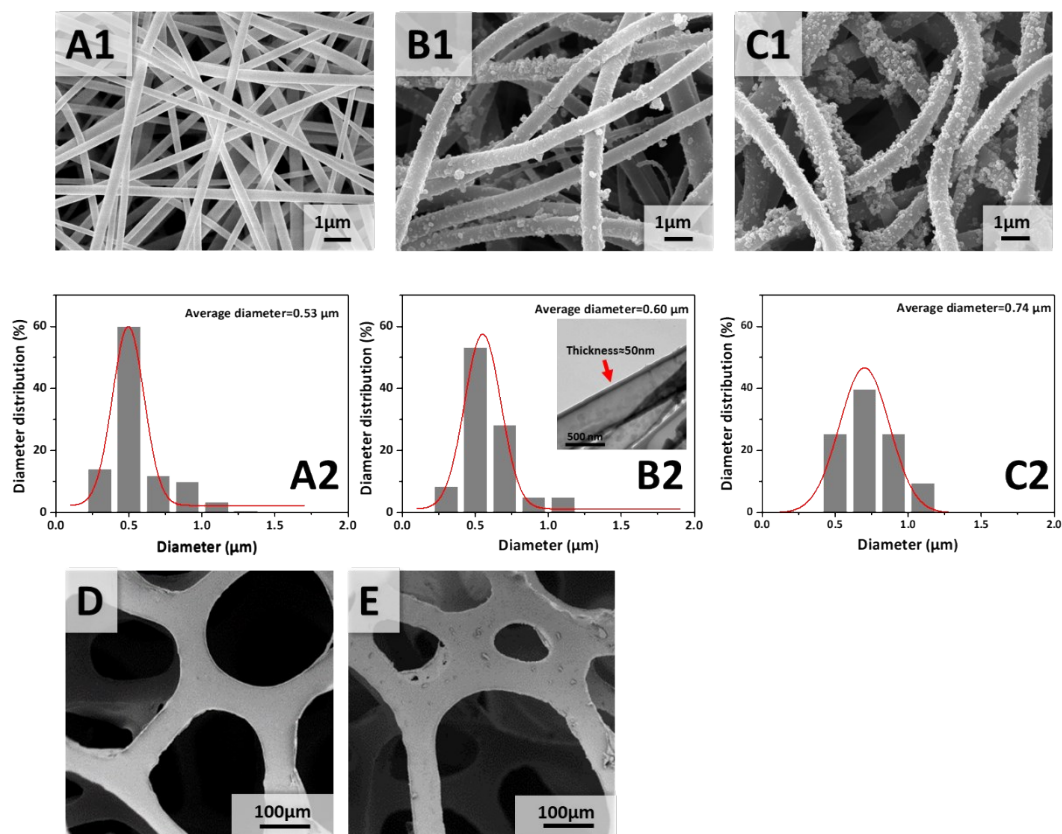
Figure S1. SEM images of (A1) PLA-NF, (B1) $PDA_{50}@NF$, (C1) $PDA_{100}@NF$, (D)PU foam and (E) PDA@PU. The diameter distribution of (A2) PLA-NF, (B2) $PDA_{50}@NF$ and (C2) $PDA_{100}@NF$. The inset in (B2) is the TEM image of PDA_{50}-t.
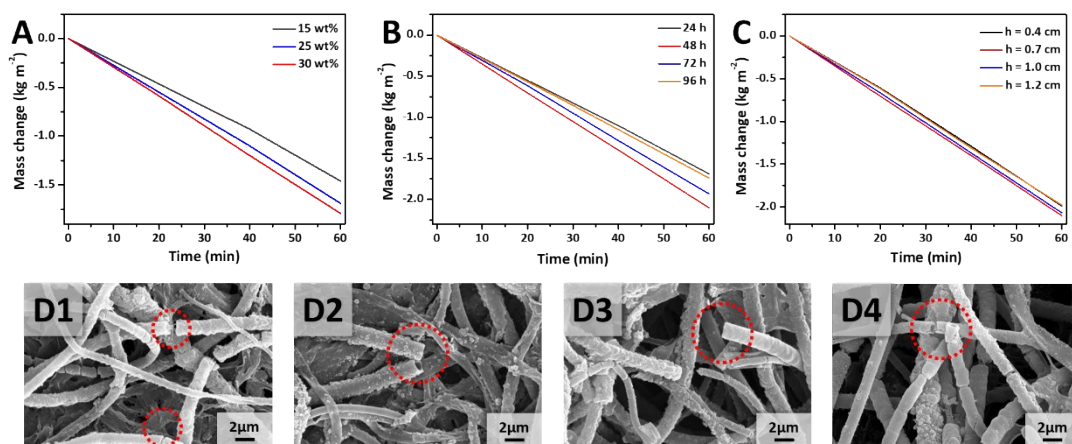

Figure S2. The mass loss of pure water for PDA_{50}-t@PU with difference of (A) the addition amount of PDA_{50}-t, (B) the time of treating $PDA_{50}@$ NF by solvent and (C) the thickness of the PU foam matrix. SEM images of PDA_{50}-t treated with different time of (D1) 24 h, (D2) 48 h, (D3) 72 h and (D4) 96 h.

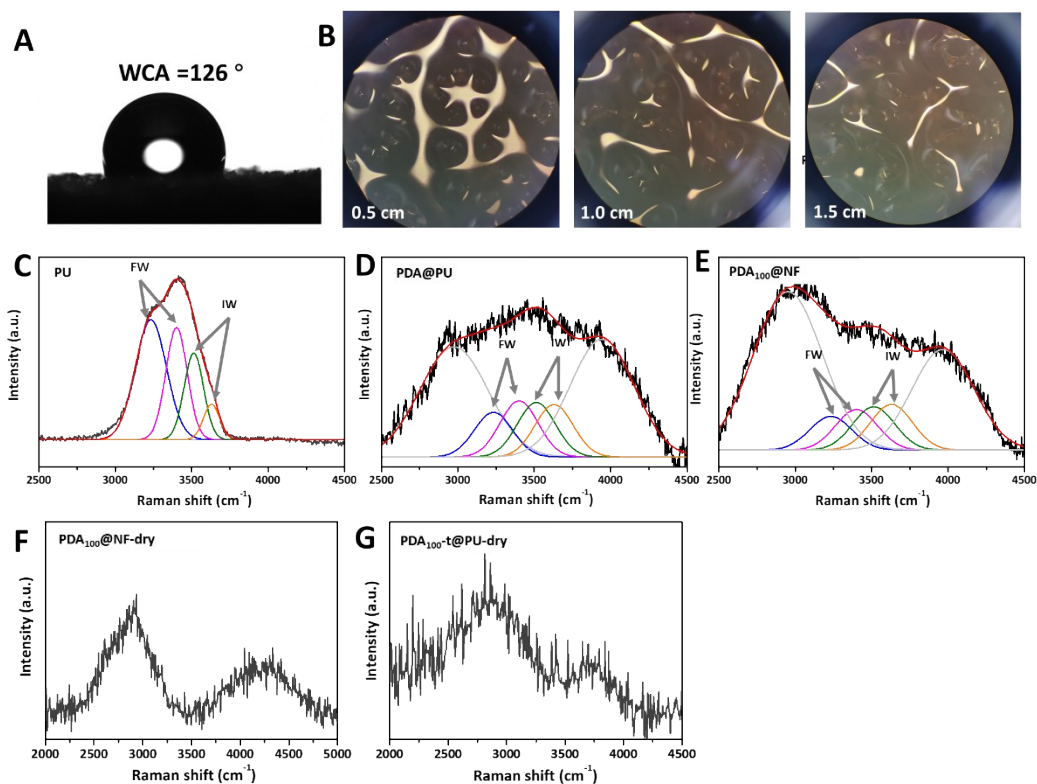## Section S2.1. Water state in various samples.

Figure S3. (A) The water contact angle (WCA) of PU foam in air. (B) Microscopy images of the water distribution at the evaporation surface of PDA@PU with different exposure height above water surface. Raman fitting curves in energy region of O-H stretching modes for water in (C) PU, (D) PDA@PU and (E) PDA$_{100}$@NF. The FW and IW represent free water and intermediate water, respectively. Raman curves of dry samples for (F) PDA$_{100}$@NF and (G) PDA$_{100}$-t@PU.

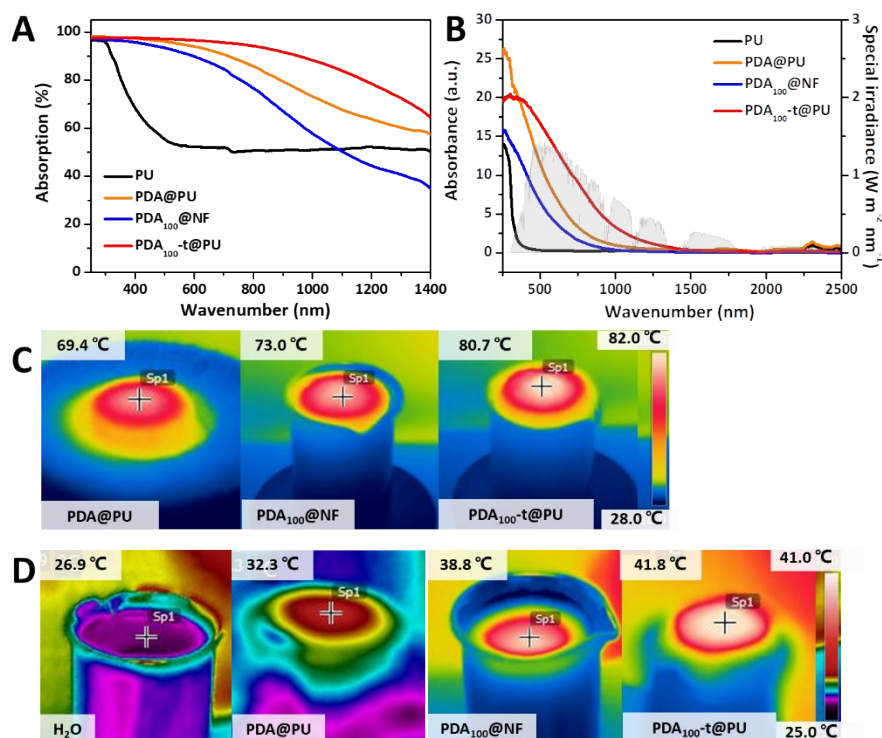## Section S2.2. Photothermal conversion performance.

Figure S4. (A) Absorption and (B) absorbance of different samples ranging from 250 to 2500 nm. The normalized spectral solar irradiance density of air mass 1.5 global (AM 1.5 G) tilt solar spectrum is shown by the blue area. Infrared images of (C) dry samples and (D) wetted samples under 1 sun.

Section S2.3. Solar vapour generation properties.

Section S2.3.1. Solar vapour generation properties of PDA$_{50}$-t@PU.

The water evaporation enthalpy and equivalent enthalpy in pure water and PDA$_{50}$-t@PU with different treatment time was measured by DSC and dark experiment (**Figure S7**A-D). Compared with pure water, the water evaporation enthalpy calculated from DSC and equivalent enthalpy of water in PDA$_{50}$-t@PUs all decreased to varying degrees. The SVG rate and the corresponding energy efficiency are shown in **Figure S7**E, the SVG rate of PDA$_{50}$-t$_{48}$@PU is 2.1 kg m^{-2} h^{-1} with the energy efficiency of 82%. In addition, although the SVG rate of PDA$_{50}$-t$_{24}$-PU is low, the higher energy efficiency is mainly attributed to the higher equivalent evaporation enthalpy and higher energy demand.
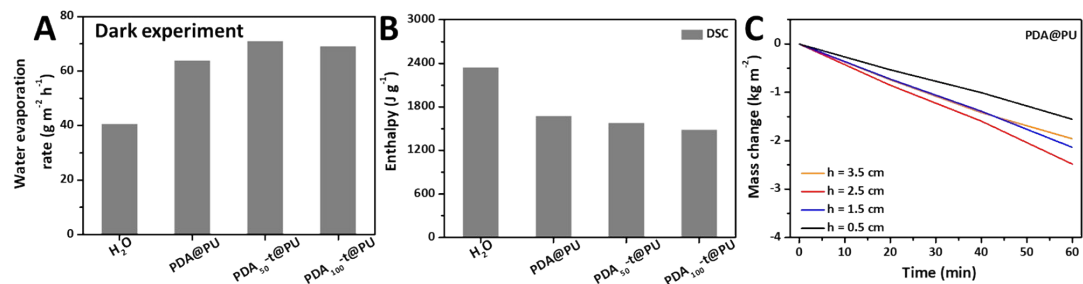
Figure S5. (A)The water evaporation rate of the pure water and samples calculated by dark experiment. (B) The measured water vaporization enthalpy of bulk water and water in samples by DSC. (C) The mass loss of PDA@PU with 3D structure under 1sun.
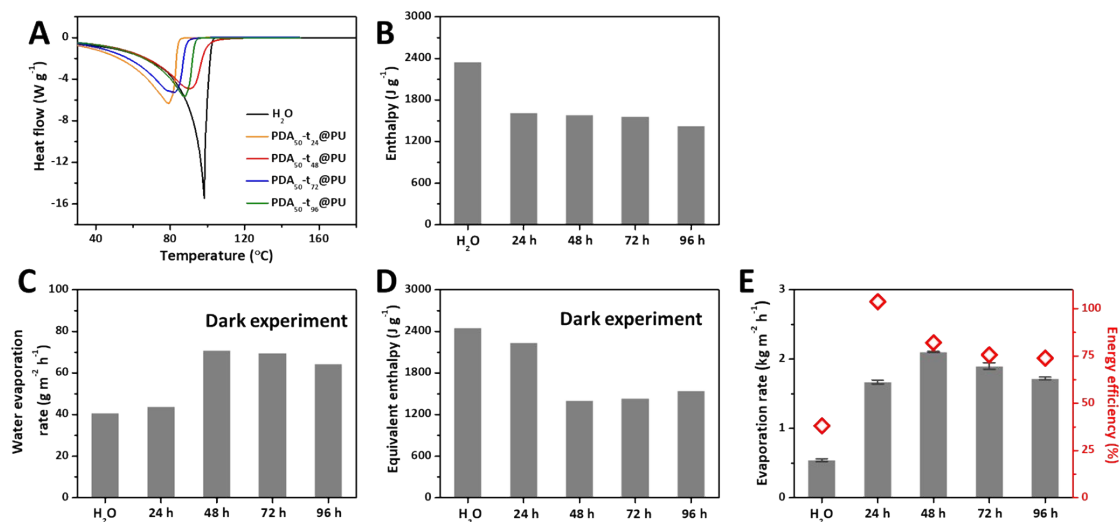

Figure S6. (A) Thermograms of the pure water and PDA$_{50}$-t@PU with different treatment time. (B) The measured water vaporization enthalpy of bulk water and water in PDA$_{50}$-t@PU via DSC. (C) The water evaporation rate and (D) equivalent enthalpy of the pure water and samples calculated in dark experiment. (E) SVG rate with corresponding energy efficiency of samples under 1 sun.

Table S1 Formula for simulated seawater

Components of simulated seawater	Adding amount	Components of simulated seawater	Adding amount
H_2O	1 L	$NaHCO_3$	0.201 g
NaCl	24.53 g	KBr	0.101 g
$MgCl_2 \cdot 6H_2O$	11.09 g	H_3BO_3	0.027 g
Na_2SO_4	4.09 g	$SnCl_2 \cdot 6H_2O$	0.042 g
$CaCl_2$	1.16 g	NaF	0.003 g
KCl	0.695 g		

Section S2.3.2. Mechanism of the environmental energy enhanced solar vapor generation.

Three energy flows were included in the heat transfer process of solar steam generation: solar energy input, steam output, and heat exchange with the environment, in the form of either energy loss to the environment or energy gain from the environment. The heat transfer process of the PDA-t@PU evaporator with different H_{aw} could be expressed as the following equations.

$$mH_{lv} = Q_t + Q_s \tag{3}$$

$$Q_t = P_{in}A_t - A_th(T_t - T_e) - \varepsilon\sigma A_t(T_t^4 - T_e^4) \tag{4}$$

$$Q_s = -A_sh(T_s - T_e) - \varepsilon\sigma A_s(T_s^4 - T_e^4) - k(T_s - T_w) \tag{5}$$

where m represents the mass flux of steam, H_{lv} represents the latent heat of water evaporation, Q_t and Q_s represent the obtained energy flux of the evaporator from the top surface and side surface, respectively, P_{in} represents the incident optical power, A_t and A_s represent the areas of the top surface and side surface, respectively, h represents the coefficient of convective heat transfer, T_t, T_e, T_s and T_w represent the temperatures of the top surface, surrounding environment, side surface and underling bulk water, respectively, ε represents the emissivity, σ represents the Stefan-Boltzmann constant, and k represents the thermal conductivity of the evaporator saturated with water. On

the basis of classical thermodynamics, when a wet object is surrounded by relatively dry air, water evaporates from the surface of the object because of the humidity gradient, which is a process of absorbing heat, thus resulting in a temperature decrease at the surface of the wet object. Furthermore, a temperature difference forms between the wet object and ambient air.

For steric evaporators with relatively large H_{aw}, the top surface is able to absorb the incident sun illumination, leading to increased temperature of the top surface. Meanwhile, the temperature of side surface of steric evaporator is lower than environmental temperature, which results in energy gains ($Q_s>0$) from the environment and promotes the steam generation process. Therefore, for steric evaporators with relatively large exposed side surface, the formula ($\eta=mE_{equ}/C_{opt}P_0$) is no longer applicable to directly calculate the corresponding energy efficiency. The actual energy input is higher than the solar energy input, resulting in energy efficiency even higher than 100% nominally.
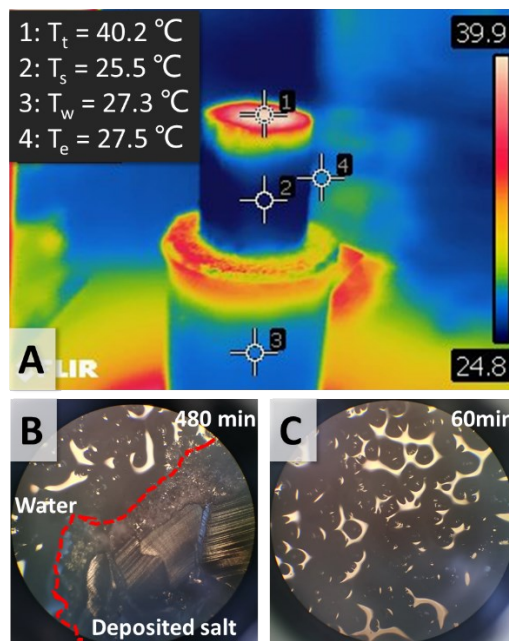

Figure S7. (A) Infrared image of cylinder shaped PDA$_{100}$-t@PU steric evaporator under 1 sun with exposure height of 3.5 cm. T_t, T_s, T_w, and T_e represent the temperatures of the top surface, side surface, underling bulk water and environment, respectively. Microscopy images of PDA$_{100}$-t@PU surface (B) with illumination for 480 min and (C) without illumination for 60 min in 10 wt% NaCl solution.